

ASMA: An Adaptive Safety Margin Algorithm for Vision-Language Drone Navigation via Scene-Aware Control Barrier Functions

Sourav Sanyal and Kaushik Roy

Electrical and Computer Engineering, Purdue University

{sanyals, kaushik}@purdue.edu

Abstract—In the rapidly evolving field of vision-language navigation (VLN), ensuring safety for physical agents remains an open challenge. For a human-in-the-loop language-operated drone to navigate safely, it must understand natural language commands, perceive the environment, and simultaneously avoid hazards in real time. Control Barrier Functions (CBFs) are formal methods that enforce safe operating conditions. Model Predictive Control (MPC) is an optimization framework that plans a sequence of future actions over a prediction horizon, ensuring smooth trajectory tracking while obeying constraints. In this work, we consider a VLN-operated drone platform and enhance its safety by formulating a novel scene-aware CBF that leverages ego-centric observations from a camera which has both Red-Green-Blue as well as Depth (RGB-D) channels. A CBF-less baseline system uses a Vision-Language Encoder with cross-modal attention to convert commands into an ordered sequence of landmarks. An object detection model identifies and verifies these landmarks in the captured images to generate a planned path. To further enhance safety, an Adaptive Safety Margin Algorithm (ASMA) is proposed. ASMA tracks moving objects and performs scene-aware CBF evaluation on-the-fly, which serves as an additional constraint within the MPC framework. By continuously identifying potentially risky observations, the system performs prediction in real time about unsafe conditions and proactively adjusts its control actions to maintain safe navigation throughout the trajectory. Deployed on a Parrot Bebop2 quadrotor in the Gazebo environment using the Robot Operating System (ROS), ASMA achieves 64%–67% increase in success rates with only a slight increase (1.4%–5.8%) in trajectory lengths compared to the baseline CBF-less VLN.

I. INTRODUCTION

Foundational models pretrained on exa-scale internet data have made significant strides in vision and language processing tasks with little to no fine-tuning, as exemplified by a new family of AI models such as BERT [1], GPT-3 [2], GPT-4 [3], CLIP [4], DALL-E [5], and PALM-E [6]. The fusion of vision and language models [4], [6] has enabled machines to interact with operating environments in increasingly intuitive ways. As VLN models become more widespread, the once sci-fi dream of robots understanding and interacting in complex environments through natural language commands is now a reality. This has been enabled by the emerging field of vision-language navigation (VLN) [7]–[12]. Autonomous drones, pivotal in smart agriculture, search and rescue, and firefighting [13], are set to contribute up to \$54.6 billion to the global economy by 2030 [14]. Imagine a scenario where VLN powered drones translate human-specified contextual instructions into actions. However, for VLN, navigating

dynamic environments using robot vision remains an open research problem. To that effect, Control Barrier Functions (CBFs) [15], [16] provide a formal mathematical framework for enforcing safe operating conditions in dynamical systems, making them useful for real-time applications where safety is crucial. On the other hand, Model Predictive Control (MPC) is an optimization framework that plans a sequence of future actions over a prediction horizon to ensure smooth trajectory tracking while obeying constraints.

In this work, we address the critical challenge of ensuring safe VLN for human-in-the-loop drone operations by introducing a novel Adaptive Safety Margin Algorithm (ASMA). Our approach integrates high-level vision-language reasoning with low-level safety-critical control methods to significantly enhance drone navigation safety. We start with a baseline system that employs a Vision-Language Encoder using cross-modal attention [17], which translates natural language commands into an ordered sequence of landmarks, verified by an object detection model (YOLOv5) [18]. To robustify navigation against dynamic environmental hazards, we formulate a novel scene-aware CBF that processes real-time ego-centric observations from an RGB-D camera. ASMA dynamically adjusts the drone’s control actions by tracking moving objects, predicting potential safety risks, and incorporating scene-aware CBF constraints within an MPC framework. By continuously identifying potentially risky observations, the system predicts unsafe conditions in real time and proactively adjusts its control actions to maintain safe navigation throughout the trajectory. The proposed integration of VLN with CBFs provides a formal safety layer which enhances VLN reliability of physical agents (in this work a drone). Our main contributions are:

- We implement a vision-language encoder using cross-modal attention and object detection to serve as a planning agent (Section III-A).
- We propose scene-aware CBFs (SA-CBFs) that adjust drone actions for improving robustness against dynamic obstacles (Section III-B).
- We integrate the entire system using Robot Operating System (ROS) to provide a full-stack modularized framework (Section III-C).
- Our detailed analysis shows significant improvements in navigation accuracy and safety when ASMA is applied to a baseline CBF-less VLN method on a Parrot Bebop2 quadrotor in ROS-Gazebo [19] (Section IV).

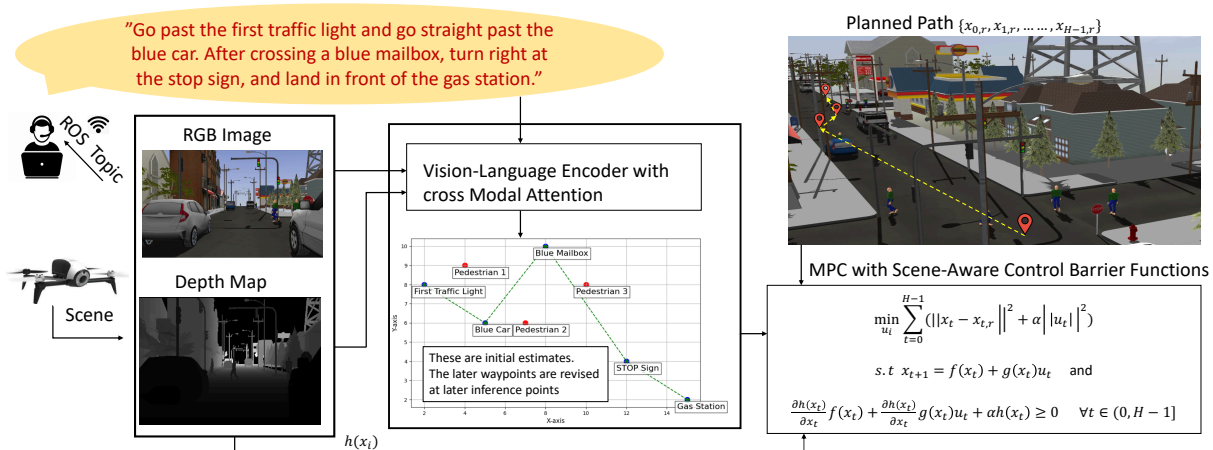


Fig. 1. Overview of the proposed ASMA framework. The system takes natural language instructions and processes RGB and depth data to create a 2D map with language-grounded landmarks and dynamic obstacles. A planned path is generated, and MPC with Scene-Aware Control Barrier Functions (CBFs) ensures safe navigation along the trajectory.

In simulation, ASMA achieves 64%–67% increase in success rates with only a slight (1.4%–5.8%) increase in trajectory lengths compared to the baseline CBF-less VLN.

II. RELATED WORK

Vision-Language Models for Robot Navigation: In Vision-Language Navigation (VLN), agents interpret language commands to navigate through environments using visual cues [7]–[12]. Previous works, such as [8], [9], have expanded VLN into continuous environments (VLN-CE). Works in [10]–[12] have explored VLN focusing on interpreting visually-grounded instructions and developing models like VLN BERT to improve navigation performance through entity-landmark pre-training techniques. [20] employs 2D LiDAR for safer waypoint prediction in VLN-CE, while [21], [22] integrate pretrained visual-language features with navigation maps. The work in [23] utilizes action prompts for improved spatial navigation precision. Room2Room [24] enables teleoperated communication using augmented reality, and [25] introduces the ‘Tryout’ method to prevent collision-related navigational stalls. However, these approaches do not address the physical dynamics of robots, crucial for verifying safety. Our work focuses on a teleoperated drone similar to [26] with VLN capabilities, utilizing an RGB-D sensor and aims to enhance its safety and reliability in dynamic environments.

Control Barrier Functions for Safety: Control barrier functions (CBFs) are essential tools from robust control theory, ensuring safety constraints are maintained in dynamic systems [15], [16]. By defining safe boundaries through mathematical functions, CBFs dynamically adjust control actions to prevent safety violations. Vision-based control barrier functions (V-CBFs) [27] extend these safety protocols to unknown environments, using conditional generative adversarial networks (C-GAN). Differentiable control barrier functions (dCBFs) integrated into neural

networks via BarrierNet [28] offer end-to-end trainable safety layers adaptable to environmental changes. Additionally, [29] develops a low-cost method for synthesizing quadratic CBFs over point cloud data, improving safe navigation. The work in [30] supports precise drone landing safety.

Although there exists several datasets and benchmarks for VLN, they do not take into account environmental changes which requires online re-planning. Furthermore, the main aim in this work is not to compete with them, but to investigate the safety aspect of VLNs by synthesizing scene-aware CBFs on the fly. To that effect this work considers two environments build from scratch using gazebo and is tested on a parrot bebop2 quadrotor by considering the necessary robot-environment dynamics required for simulating and testing the safety and reliability challenges associated with agentic VLNs in a physical world.

III. PROPOSED APPROACH

In this work, we deploy the Parrot Bebop 2 quadrotor in a ROS-powered Gazebo environment (following [31]–[33]) with an RGB-D sensor. We introduce ASMA—an Adaptive Safety Margin Algorithm for drone VLN (see Figure 1). The system processes natural language instructions alongside RGB and depth data via a Vision-Language Encoder with cross-modal attention, which extracts semantic and spatial features to build a language-grounded 2D map of landmarks and obstacles. A planned path is then generated, and a control policy using MPC with Scene-Aware CBFs ensures safe navigation while adapting to environmental changes.

A. Vision-Language Encoder with Cross-Modal Attention

Figure 2 illustrates our proposed pipeline for grounding language instructions in detected visual objects. We leverage a CLIP-based joint embedding space and YOLOv5 detections to identify and order landmarks specified in the instruction.

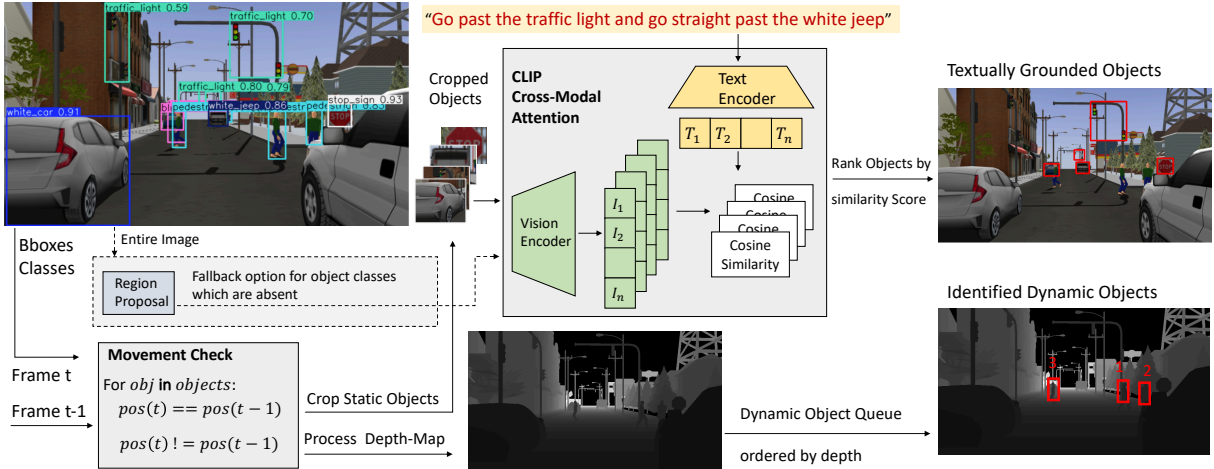


Fig. 2. Illustration of the multi-modal cross-attention pipeline for text-conditioned navigation. The system first detects objects using YOLOv5, followed by a movement check to classify static and dynamic objects across frames. Static objects are cropped and fed into a CLIP-based cross-modal attention module, which ranks objects based on textual relevance. For dynamic objects, a depth map is used to sort them by distance, enabling downstream obstacle-aware planning. A fallback mechanism is included to handle objects not recognized by YOLO, using region proposals and CLIP-based zero-shot recognition.

Before processing the instruction, we briefly perform a movement check to differentiate dynamic from static objects. For each detected object, let $\text{pos}_i(t)$ denote the center of its bounding box at time t . If

$$\text{pos}_i(t) = \text{pos}_i(t-1), \quad (1)$$

the object is considered static; otherwise, if

$$\text{pos}_i(t) \neq \text{pos}_i(t-1), \quad (2)$$

the object is marked as dynamic and prioritized for collision avoidance. The static objects are then cropped and passed on to the CLIP model, whereas the dynamic objects are identified and processed from the depth-map. The depth map can be imagined as instance segmentation, enabling the drone to steer away from structures such as walls, trees, and buildings while enforcing safety. This provides complementary spatial awareness beyond the object detector, further contributing to the safety-critical information required for downstream safety-aware control (discussed later).

Given a natural language command (e.g., "Go past the first traffic light and go straight past the blue car."), we tokenize the instruction to extract a sequence of landmarks in the specified order such as traffic light (landmark #1) and blue car (landmark #2). This preserves the user-defined sequence, ensuring the drone navigates the landmarks *in the same order* they appear in the instruction. An RGB image \mathbf{I} from the drone's onboard camera is passed to YOLOv5, which outputs bounding boxes

$$\mathbf{bbox}_i = (x_1^{(i)}, y_1^{(i)}, x_2^{(i)}, y_2^{(i)}, l_i), \quad (3)$$

for $i = 1, \dots, N$. Each bounding box localizes a detected object, and we crop that region from \mathbf{I} :

$$\mathbf{I}_i^{\text{crop}} = \text{CropImage}(\mathbf{I}, \mathbf{bbox}_i). \quad (4)$$

For each landmark token (e.g., "traffic light") in the user instruction, we first encode the text query \mathbf{T}_ℓ via CLIP's text encoder:

$$\mathbf{z}_{\text{text}}^\ell = \Phi_{\text{text}}(\mathbf{T}_\ell). \quad (5)$$

Similarly, for each detected object i , we crop the corresponding bounding box and feed it to CLIP's image encoder:

$$\mathbf{z}_{\text{obj}}^i = \Phi_{\text{img}}(\mathbf{I}_i^{\text{crop}}). \quad (6)$$

We then compute the cosine similarity

$$S_{\ell,i} = \frac{\mathbf{z}_{\text{obj}}^i \cdot \mathbf{z}_{\text{text}}^\ell}{\|\mathbf{z}_{\text{obj}}^i\| \|\mathbf{z}_{\text{text}}^\ell\|}, \quad (7)$$

for all detected objects to find the most relevant match for landmark ℓ . The highest-scoring bounding box \mathbf{bbox}_{i^*} is selected if $S_{\ell,i^*} > \theta$, where θ is a predefined confidence threshold. If no bounding box exceeds the threshold θ for a landmark ℓ , a fallback mechanism is invoked: (i) lower-confidence YOLO detections or additional bounding-box candidates (region proposals) are used to estimate the landmark's location; (ii) if no suitable match is found, the system alerts the user that landmark ℓ is missing and requests a revised instruction. This strategy ensures that the planned path remains robust even when landmarks are partially visible or detected with low confidence.

Path Generation with Landmark Order: After identifying the bounding-box centers \mathbf{p}_ℓ for each landmark ℓ , we arrange these points in the precise sequence given by the user. This ordered list of waypoints defines the drone's route:

$$\mathbf{p}_1 \rightarrow \mathbf{p}_2 \rightarrow \dots \rightarrow \mathbf{p}_L,$$

where each \mathbf{p}_ℓ corresponds to a landmark in the user's instruction. A path planner then constructs a suitable trajectory by connecting these waypoints. As the drone progresses along the route, this process is invoked repeatedly, and the

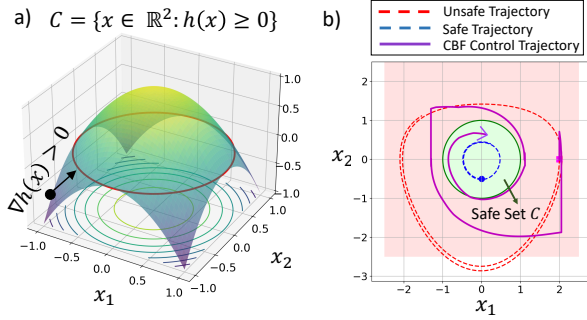


Fig. 3. Toy Illustration of Control Barrier Functions. (a) 3D view of the safe set \mathcal{C} where $h(\mathbf{x}) \geq 0$ (above red ring). (b) Comparison of trajectories: unsafe (red dashed), safe (blue dashed), and CBF-controlled (magenta solid).

waypoints are revised dynamically, as later landmarks in the instruction may become visible in the drone’s field of view. By preserving the user-defined landmark order and leveraging CLIP-based similarity scores, our cross-modal approach ensures that the drone navigates to each relevant scene element in the intended sequence and maintains safety throughout the generated path.

B. Enhancing VLN with Formal Safety Methods

Control Barrier Functions (CBFs) are essential tools in safety-critical control systems that enforce safety constraints through mathematical functions. In this work, we integrate CBFs within a Model Predictive Control (MPC) framework, ensuring that safety constraints are proactively enforced while the drone follows its planned trajectory.

1) *Preliminaries:* We consider a quadrotor described by the following non-linear control affine dynamics with an ego-centric depth-map:

$$\dot{\mathbf{x}} = f(\mathbf{x}) + g(\mathbf{x})\mathbf{u}, \quad \boldsymbol{\xi} = \Psi(\mathbf{x}, \mathbf{d}) \quad (8)$$

Here, $\dot{\mathbf{x}}$ denotes the time derivative of the state vector $\mathbf{x} \in \mathbb{R}^{12}$, covering the drone’s positions, orientations, and velocities. The control input $\mathbf{u} \in \mathbb{R}^4$, consists of thrust, roll, pitch, and yaw. Functions $f(\mathbf{x})$ form the autonomous dynamics and $g(\mathbf{x})$ signifies the dynamics that can be controlled in an affine manner. Additionally, the depth-map \mathbf{d} provides obstacle distances, with $\boldsymbol{\xi} = \Psi(\mathbf{x}, \mathbf{d})$ transforming these distances from pixel to physical space, incorporating the drone’s current position. Let $\mathcal{C} \subset \mathbb{R}^{12}$ represent a safety set defined through a continuously differentiable function $h(\mathbf{x})$ such that:

$$\mathcal{C} = \{\mathbf{x} \in \mathbb{R}^{12} : h(\mathbf{x}) \geq 0\} \quad (9)$$

Figure 3a illustrates a toy safety set \mathcal{C} , marked by the boundary where $h(\mathbf{x}) = 0$ and the region where $h(\mathbf{x}) > 0$, indicating safe operational zones. The function $h(\mathbf{x})$ is characterized by its lie derivatives:

$$L_f h(\mathbf{x}) = \nabla h(\mathbf{x}) \cdot f(\mathbf{x}), \quad (10a)$$

$$L_g h(\mathbf{x}) = \nabla h(\mathbf{x}) \cdot g(\mathbf{x}), \quad (10b)$$

which are critical for monitoring the system’s safety relative to state changes and control action changes.

Algorithm 1 Scene-Aware CBF-MPC

```

1: function SA-CBF-MPC( $\mathbf{p}_{\text{curr}}, \mathbf{X}_{\text{plan}}, h(\mathbf{x}), \text{Obstacles}$ )
2:   Formulate MPC optimization problem over horizon  $H$ 
3:   for each time step do  $t = 0$  to  $H - 1$ 
4:     Extract reference state  $\mathbf{x}_{r,t}$  from  $\mathbf{X}_{\text{plan}}$ 
5:     for each obstacle in  $\text{Obstacles}$  do
6:       Compute  $h(\mathbf{x})$  using Equation 20
7:       if  $h(\mathbf{x}) < 0$  then
8:         Apply CBF constraints to enforce safety
9:       end if
10:    end for
11:  end for
12:  Solve MPC optimization incorporating CBF constraints
13:  return optimal control sequence  $\mathbf{U} = [\mathbf{u}_0, \mathbf{u}_1, \dots, \mathbf{u}_{H-1}]$ 
14: end function

```

Theorem (Safety Verification): For safety verification, it is required that:

$$L_f h(\mathbf{x}) + L_g h(\mathbf{x})\mathbf{u} + \alpha(h(\mathbf{x})) \geq 0, \quad (11)$$

where α is a class \mathcal{K} function (meaning $\alpha(0) = 0$ and $\alpha(\mathcal{K}x_2) > \alpha(\mathcal{K}x_1) \forall x_2 > x_1$ and $\mathcal{K} > 0$). $\nabla h(\mathbf{x}) > 0$ in the unsafe region ($h(\mathbf{x}) < 0$) will drive $h(\mathbf{x})$ to become positive again.

Corollary (CBF-MPC Integration): If a function $h(\mathbf{x})$ can be designed such that adjustments in \mathbf{u} satisfy the constraint in Eqn. (11) at every time step, then embedding these constraints inside an MPC framework ensures that the system guarantees safety while optimizing trajectory tracking.

This forms the core of our Scene-Aware CBF-MPC framework (Algorithm 1), where the safety constraint is included as part of the trajectory optimization problem, rather than being enforced in a purely reactive manner.

$$\min_{\mathbf{u}_0, \dots, \mathbf{u}_{H-1}} J = \sum_{t=0}^{H-1} \left\{ \|\mathbf{x}_t - \mathbf{x}_{r,t}\|^2 + \alpha\|\mathbf{u}_t\|^2 \right\}, \quad (12)$$

subject to:

$$\mathbf{x}_{t+1} = f(\mathbf{x}_t) + g(\mathbf{x}_t)\mathbf{u}_t, \quad \forall t \in (0, H - 1] \quad (13)$$

$$L_f h(\mathbf{x}_t) + L_g h(\mathbf{x}_t)\mathbf{u}_t + \alpha(h(\mathbf{x}_t)) \geq 0, \quad \forall t \in (0, H - 1] \quad (14)$$

$$\begin{aligned} & \Rightarrow \underbrace{\frac{\partial h(\mathbf{x}_t)}{\partial \mathbf{x}_t} f(\mathbf{x}_t) + \frac{\partial h(\mathbf{x}_t)}{\partial \mathbf{x}_t} g(\mathbf{x}_t)\mathbf{u}_t}_{\text{Expanded form of Lie derivatives}} \\ & \quad + \alpha h(\mathbf{x}_t) \geq 0, \quad \forall t \in (0, H - 1] \end{aligned} \quad (15)$$

where $\mathbf{x}_{r,t}$ denotes the reference trajectory computed from waypoints extracted by the vision-language encoder.

To incorporate the outputs of our vision-language pipeline and the depth sensor into the control loop, we convert pixel-level detections into 3D positions in the drone’s reference frame and then into the global frame. Specifically, for pixel coordinates (i, j) in the cropped depth map, we retrieve the depth value d . Using the intrinsic parameters (focal length f

and camera center (c_x, c_y) , we obtain the 3D coordinates in the camera frame:

$$X_c = (i - c_x) \cdot \frac{d}{f}, \quad Y_c = (j - c_y) \cdot \frac{d}{f}, \quad Z_c = d. \quad (16)$$

These coordinates are then transformed into the global frame:

$$\begin{bmatrix} X_g \\ Y_g \\ Z_g \end{bmatrix} = \mathbf{R} \cdot \begin{bmatrix} X_c \\ Y_c \\ Z_c \end{bmatrix} + \vec{\mathbf{p}}_{\text{curr}}, \quad (17)$$

where \mathbf{R} is the rotation matrix representing the drone's current heading, and $\vec{\mathbf{p}}_{\text{curr}}$ is the drone's estimated global position. An Extended Kalman Filter (EKF) [34] updates both \mathbf{R} and $\vec{\mathbf{p}}_{\text{curr}}$ in real time, mitigating sensor drift.

Our vision-language detection module provides bounding boxes for both targets and obstacles. We take each bounding box center (i, j) , retrieve its corresponding depth d , and convert it to global coordinates $\vec{\mathbf{p}}_{\text{target}}$ or $\vec{\mathbf{p}}_{\text{obs}}$ via the above transformation.

Let $\vec{\mathbf{p}}_{\text{target}}$ be the 3D position of the intended waypoint and $\vec{\mathbf{p}}_{\text{obs}}$ the position of an obstacle. We define

$$\vec{\mathbf{d}}_{\text{target}} = \vec{\mathbf{p}}_{\text{target}} - \vec{\mathbf{p}}_{\text{curr}}, \quad \vec{\mathbf{d}}_{\text{obs}} = \vec{\mathbf{p}}_{\text{obs}} - \vec{\mathbf{p}}_{\text{curr}}.$$

Obstacles are prioritized by

$$\text{Priority} = \frac{1}{\|\vec{\mathbf{d}}_{\text{obs}}\|}, \quad (18)$$

so closer obstacles are processed first. If a priority obstacle is on a collision course, our Scene-Aware CBF yields

$$\sigma_d = \text{sign}\left(\left(\vec{\mathbf{d}}_{\text{target}} \times \vec{\mathbf{d}}_{\text{obs}}\right)_z\right) \quad (19)$$

which indicates whether an obstacle lies to the right ($\sigma_d > 0$) or left ($\sigma_d < 0$) of the target direction. This σ_d is then used in Equation (22a) to assign the correct sign to the gradient $\frac{\partial h(\mathbf{x})}{\partial \mathbf{x}}$, ensuring appropriate lateral steering to avoid obstacles.

2) **Scene-Aware CBF**: The proposed Scene-Aware CBF which is used within the MPC framework is defined as:

$$h(\mathbf{x}) = \begin{bmatrix} \vec{\mathbf{d}}_{\text{obs}} - \mathbf{d}_{\text{safe}} \\ \theta - \theta_{\text{safe}} \end{bmatrix} \quad (20)$$

$$\theta = \cos^{-1}\left(\frac{\vec{\mathbf{d}}_{\text{target}} \cdot \vec{\mathbf{d}}_{\text{obs}}}{\|\vec{\mathbf{d}}_{\text{target}}\| \|\vec{\mathbf{d}}_{\text{obs}}\|}\right), \quad (21)$$

where θ is the angle between $\vec{\mathbf{d}}_{\text{obs}}$ and $\vec{\mathbf{d}}_{\text{target}}$. The gradient for each component of $h(\mathbf{x})$ is given by:

$$\frac{\partial h_1(\mathbf{x})}{\partial \mathbf{x}} = \sigma_d \frac{\partial \vec{\mathbf{d}}_{\text{obs}}}{\partial \mathbf{x}}, \quad (22a)$$

$$\frac{\partial h_2(\mathbf{x})}{\partial \mathbf{x}} = -\csc \theta \frac{\partial \cos \theta}{\partial \mathbf{x}}. \quad (22b)$$

These gradient expressions feed into the Lie derivatives in Eq. (11), guiding the optimizer to adjust the control actions for safety. When multiple obstacles are present, the system employs a priority queue to process them in ascending order of $\|\vec{\mathbf{d}}_{\text{obs}}\|$. This ensures that obstacles closest to the drone receive immediate attention.

Algorithm 2 Adaptive Safety Margin Algorithm (ASMA)

Input: RGB-D image \mathbf{I} , VLN instruction cmd

Output: Drone command vector \mathbf{u} with safety constraints

```

1: Initialize global_image, global_depth from RGB-D
2: while not ROSPY.IS_SHUTDOWN() do
3:    $\mathbf{L} \leftarrow \text{ExtractLandmarks}(\text{cmd})$  ▷ Tokenize instruction
4:   Start Thread A:
5:     Acquire image_lock ▷ Wait for  $\mathbf{I}$ 
6:      $\text{bbox} \leftarrow \text{DetectRelevantObjects}(\text{global\_img}, \mathbf{L})$ 
7:      $\mathbf{I}_{\text{crop}} \leftarrow \text{CropObjects}(\text{global\_img}, \text{bbox})$ 
8:      $\mathbf{D}_{\text{crop}} \leftarrow \text{CropDepth}(\text{global\_depth}, \text{bbox})$ 
9:     Release image_lock
10:  Start Thread B:
11:    Acquire image_lock ▷ Wait for  $\mathbf{I}$  and cropped objects
12:     $\mathbf{E}_{\text{objs}} \leftarrow \Phi_{\text{img}}(\mathbf{I}_{\text{crop}})$ 
13:     $\mathbf{E}_{\text{text}} \leftarrow \Phi_{\text{text}}(\mathbf{L})$ 
14:     $\mathbf{S} \leftarrow \text{ComputeSimilarity}(\mathbf{E}_{\text{objs}}, \mathbf{E}_{\text{text}})$ 
15:    Release image_lock
16:     $\mathbf{X}_{\text{plan}} \leftarrow \text{GeneratePath}(\mathbf{L}, \text{bbox}, \mathbf{D}_{\text{crop}})$ 
17:    if any  $\mathbf{L}$  not in detected object classes then
18:       $\text{bbox}_{\text{fallback}} \leftarrow \text{RegionProposal}(\text{global\_img})$ 
19:       $\mathbf{X}_{\text{plan}} \leftarrow \text{UpdatePath}(\mathbf{X}_{\text{plan}}, \text{bbox}_{\text{fallback}})$ 
20:    end if
21:     $\mathbf{u} \leftarrow \text{SA-CBF-MPC}(\vec{\mathbf{p}}_{\text{curr}}, \mathbf{X}_{\text{plan}}, h(\mathbf{x}), \{\vec{\mathbf{p}}_{\text{obs}}\})$ 
22:    PUBLISH_CONTROL( $\mathbf{u}$ )
23: end while

```

C. Adaptive Safety Margin Algorithm (ASMA)

Algorithm 2 gives a walkthrough of the entire system. Each iteration begins by tokenizing the VLN instruction (line 3). Thread A locks the image buffer (line 5), detects objects (line 6), and crops RGB and depth data (lines 7–8). Meanwhile, Thread B computes similarity scores between the cropped objects and instruction tokens (lines 12–15). A planning module then generates a trajectory using these detections (line 17), invoking a fallback if landmarks are missing (lines 18–20). Finally, the planned trajectory is passed to the SA-CBF-MPC module (line 21), which enforces safety and publishes the control command (line 22). This process repeats continuously.

IV. RESULTS

A. Methodology

We implemented the ASMA framework in ROS on a parrot bebop2 quadrotor within the Gazebo environment. The pretrained CLIP model was obtained from OpenAI's repository [17]. Object detection was performed using YOLOv5 [18] (~21 million parameters), with training data annotated via LabelImg [35]. The pretrained CLIP consisted of ~149 million parameters. Because of the large model sizes, we performed thread synchronization (Algorithm 2) to toggle between the two inference modes. The threshold θ in Vision-Language Encoder was set to 0.2. Scene-Aware CBF with MPC optimizations sampled at 5 Hz (to give sufficient time to the Vision-Language Encoder) were conducted using `cvxopt` [36], and the RotorS simulator [37] was used to integrate lower level control. $\vec{\mathbf{d}}_{\text{safe}}$ was set to 2 meters and θ_{safe} to 30 degrees. RGB-D focal length f was 10 meters.

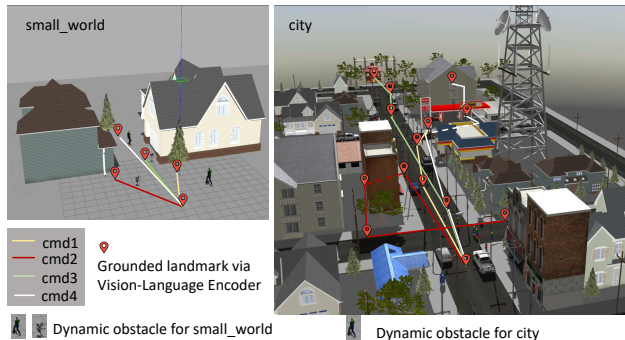


Fig. 4. Gazebo environments – *left: small_world*, *right: city*

TABLE I
VISION-LANGUAGE ENCODER PERFORMANCE.

Environment	Average Similarity Score	Grounding Accuracy (%)
small_world	0.36	98
city	0.31	92

B. Comparative Schemes

- **CBF-less VLN:** A baseline vision-language navigation (VLN) method without safety enforcement through control barrier functions (CBFs).
- **ASMA-Reactive:** Implements scene-aware CBFs based on the constraint in Equation (11), enforcing safety reactively. The nominal control here is a basic PID.
- **ASMA-MPC:** Integrates CBF constraints within a model-predictive control (MPC) framework for anticipatory safety enforcement.
- **CBF-Only Navigation:** Uses CBF constraints for collision avoidance but does not incorporate vision-language grounding. This is basically the oracle which assumes obstacle pose information from ground-truth.

We test our method in two simulated environments (Figure 4): the *small world* for the CBF-based MPC formulation and the more complex and cluttered *city* environment for planning (Table II). In *city*, commands include flying through a narrow alley (**cmd2**), entering a gazebo and landing (**cmd3**), and ascending to a third-floor balcony to land (**cmd4**), all requiring spatial reasoning. See the additional media file for simulations. Performance is evaluated using Trajectory Length (TL), Success Rate (SR; trials reaching within 1 meter of the target), and Navigation Error (NE; the final Euclidean distance from the target).

C. Vision-Language Encoder Performance

We evaluate our vision-language encoder by computing cosine similarity scores between the CLIP-encoded text queries and embeddings of cropped object regions. This includes the object detector’s supervised landmark classification as well as the fall-back region-proposal based landmark identification. Grounding accuracy is defined as the percentage of landmarks correctly matched with detected objects.

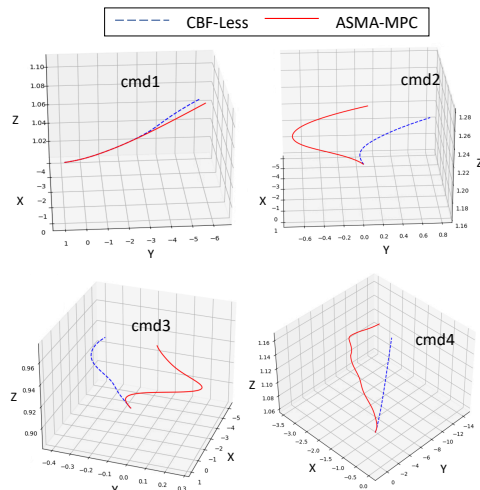


Fig. 5. Comparison of navigation trajectories for four VLN instructions in the *small world* environment. The blue dashed line represents the **CBF-less** method, while the red solid line corresponds to **ASMA-MPC**.

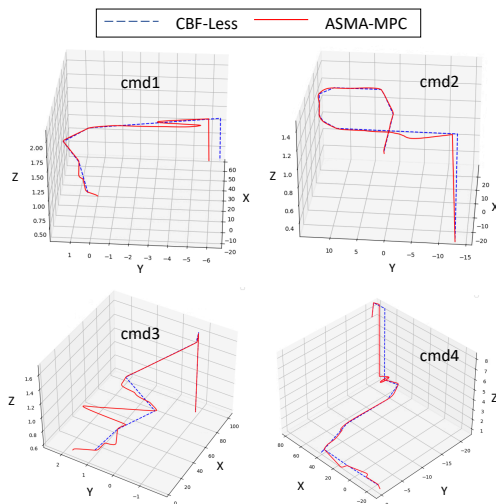


Fig. 6. Comparison of navigation trajectories for four VLN instructions in the *city* environment. The blue dashed line represents the **CBF-less** method, while the red solid line corresponds to **ASMA-MPC**.

Table I summarizes the encoder’s quantitative performance for the *small_world* and *city* environments. Note that these similarity measures are obtained in a zero-shot manner, without any fine-tuning, as a consequence of querying a large vision-language model with another object detector model. Although fine-tuning could boost similarity scores, our goal is landmark extraction. Fine-tuning would reduce generalization and narrow the model’s scope. These results demonstrate that our encoder efficiently grounds language tokens to visual landmarks, providing essential information for downstream safety-aware control.

D. Vision-Language Navigation Performance

Table II compares the VLN performance of four methods in the *small_world* (upper) and *city* (lower) environ-

TABLE II
VLN PERFORMANCE IN TWO ENVIRONMENTS. ↓ INDICATES LOWER IS BETTER. ↑ IMPLIES HIGHER IS BETTER.

Environment	VLN Instruction	Metric	CBF-Less	ASMA-Reactive	ASMA-MPC	CBF-Only
small_world	cmd1: Go to the house on the left.	TL ↓	8.54	8.60	8.40	8.52
		SR ↑	61.01	92.19	95.32	91.82
		NE ↓	2.80	3.11	2.40	2.40
	cmd2: Go to the tree on the right.	TL ↓	4.64	5.41	5.10	4.85
		SR ↑	55.59	90.08	93.80	92.49
		NE ↓	1.21	1.23	1.00	0.96
	cmd3: Find the mailbox, and fly towards it.	TL ↓	5.24	6.17	5.98	6.27
		SR ↑	55.32	91.18	94.21	91.47
		NE ↓	2.01	2.01	1.83	1.83
	cmd4: Fly between the two houses, look for a tree, and fly towards it.	TL ↓	14.51	14.70	13.90	18.82
		SR ↑	50.81	91.41	96.02	93.03
		NE ↓	0.51	0.50	0.35	0.36
city	cmd1: Go past the first traffic light and go straight past the blue car. After crossing a blue mailbox, turn right at the stop sign, and land in front of the gas station.	TL ↓	86.37	89.50	89.30	87.12
		SR ↑	58.32	88.90	94.45	90.10
		NE ↓	3.20	3.40	2.90	3.10
	cmd2: Follow the road. After the crossing, fly through the alley before the blue mailbox. Turn left, pass between buildings, turn left at the oak tree, and if a white truck is visible, land in front of it.	TL ↓	118.60	129.19	112.83	126.15
		SR ↑	52.25	87.30	93.21	89.99
		NE ↓	1.60	1.50	1.25	1.30
	cmd3: Head past the second traffic light. If an ambulance is on the left, fly past it and the stop sign. Enter the gazebo and land inside.	TL ↓	169.80	179.70	172.29	174.80
		SR ↑	54.10	89.50	94.12	90.55
		NE ↓	2.40	2.10	1.80	1.95
	cmd4: Fly past the first traffic light, then turn right before the gas station. Before the white truck, turn left. At the apartment with stairs, ascend to the third floor and land inside the hallway.	TL ↓	139.10	143.70	140.02	147.39
		SR ↑	48.92	89.60	95.42	91.80
		NE ↓	0.70	0.60	0.50	0.55

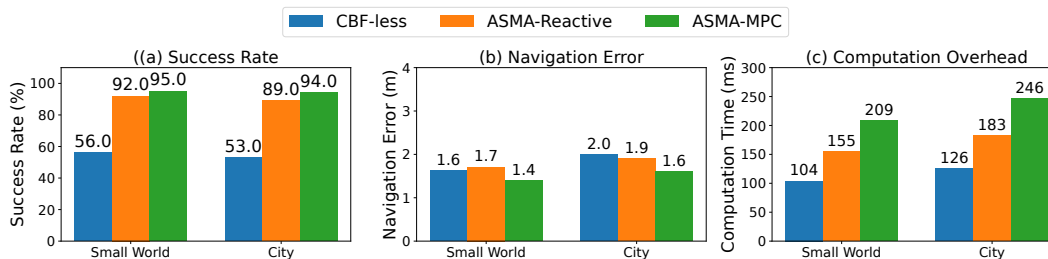


Fig. 7. Ablation study results comparing the three methods (CBF-less, ASMA-Reactive, and ASMA-MPC) across two environments (Small World and City). Bars indicate average Success Rate (SR), Navigation Error (NE), and Computation Time for 1 inference cycle.

ments. In *small world*, the baseline CBF-less approach yields lower Success Rates (SR), while ASMA-Reactive and ASMA-MPC significantly boost SR (up to 96.02%). ASMA-Reactive sometimes increases Trajectory Length (TL), whereas ASMA-MPC balances higher SR with moderate TL. CBF-Only also surpasses the baseline but lacks vision–language grounding for task-focused navigation. In *city*, which features more complex instructions and dynamic obstacles, the baseline again shows low SR, while ASMA-Reactive offers substantial gains. ASMA-MPC further anticipates hazards, improving SR up to 95.42% and relatively low Navigation Error (NE). Figures 5 and 6 illustrate representative trajectories: the CBF-less method (dashed blue) often nears obstacles or fails to reach the goal, whereas ASMA-MPC (solid red) maintains safer paths and completes instructions more reliably. Compared to CBF-less VLN, ASMA-Reactive and ASMA-MPC improved success rates by 64.1% and 67.5% on average, with 1.4% - 5.8% trajectory increases due to safety detours.

E. Ablation Study

Our ablation study evaluates three variants—CBF-less, ASMA-Reactive, and ASMA-MPC—in both small world and

city environments. As shown in Figure 7, CBF-less suffers from low success rates, while ASMA-Reactive and ASMA-MPC improve success rates, with ASMA-MPC further enhancing them by proactively enforcing safety constraints. ASMA-MPC achieves the lowest navigation error, though it incurs higher computational overhead due to the integrated MPC and CBF constraints. This additional cost, increasing processing time by roughly 30–40%, is justified by improved safety and accuracy, while still meeting real-time requirements on an Intel Core i9 with an NVIDIA GeForce RTX 3090 (2 GB). Further optimizations on dedicated hardware accelerators are needed for onboard embedded deployment.

V. SUMMARY

In this work, we introduced ASMA (Adaptive Safety Margin Algorithm) to enhance VLN safety for drones using a novel scene-aware CBF formulation. ASMA dynamically adjusts control actions based on real-time depth data, ensuring safe navigation in complex environments. Compared to a baseline CBF-less VLN model, ASMA-Reactive and ASMA-MPC improved success rates significantly, with minor trajectory increases due to safety detours. Our approach uses object detection for landmarks and obstacle avoidance and

instance segmentation (via depth-maps) to maintain safe distances. Alternatives like semantic segmentation could further enhance navigation in situations where clear navigation path is not visible. ASMA can be extended to various perception modalities, hence serving as a general framework for scene-aware CBFs in enhancing VLN safety.

VI. ACKNOWLEDGEMENT

This work was supported by the Center for the Co-Design of Cognitive Systems (CoCoSys), a center in JUMP 2.0, an SRC program sponsored by DARPA.

REFERENCES

- [1] J. Devlin, “Bert: Pre-training of deep bidirectional transformers for language understanding,” *arXiv preprint arXiv:1810.04805*, 2018.
- [2] T. Brown, B. Mann, and et al., “Language models are few-shot learners,” *Advances in Neural Information Processing Systems*, vol. 33, pp. 1877–1901, 2020.
- [3] J. Achiam, S. Adler, S. Agarwal, L. Ahmad, I. Akkaya, F. L. Aleman, D. Almeida, B. Altenschmidt, S. Altman, S. Anadkat et al., “Gpt-4 technical report,” *arXiv preprint arXiv:2303.08774*, 2023.
- [4] A. Radford, J. W. Kim, C. Hallacy, A. Ramesh, G. Goh, S. Agarwal, G. Sastry, A. Askell, P. Mishkin, J. Clark et al., “Learning transferable visual models from natural language supervision,” in *International conference on machine learning*. PMLR, 2021, pp. 8748–8763.
- [5] A. Ramesh, M. Pavlov, G. Goh, S. Gray, C. Voss, A. Radford, M. Chen, and I. Sutskever, “Zero-shot text-to-image generation,” in *International conference on machine learning*. Pmlr, 2021, pp. 8821–8831.
- [6] D. Driess, F. Xia, M. S. Sajjadi, C. Lynch, A. Chowdhery, B. Ichter, A. Wahid, J. Tompson, Q. Vuong, T. Yu et al., “Palm-e: An embodied multimodal language model,” *arXiv preprint arXiv:2303.03378*, 2023.
- [7] D. Shah, B. Osiński, S. Levine et al., “Lm-nav: Robotic navigation with large pre-trained models of language, vision, and action,” in *Conference on robot learning*. PMLR, 2023, pp. 492–504.
- [8] J. Krantz, E. Wijmans, A. Majumdar, D. Batra, and S. Lee, “Beyond the nav-graph: Vision-and-language navigation in continuous environments,” in *Computer Vision—ECCV 2020: 16th European Conference, Glasgow, UK, August 23–28, 2020, Proceedings, Part XXVIII 16*. Springer, 2020, pp. 104–120.
- [9] Y. Hong, Z. Wang, Q. Wu, and S. Gould, “Bridging the gap between learning in discrete and continuous environments for vision-and-language navigation,” in *Proceedings of the IEEE/CVF Conference on Computer Vision and Pattern Recognition*, 2022, pp. 15 439–15 449.
- [10] P. Anderson, Q. Wu, D. Teney, J. Bruce, M. Johnson, N. Sünderhauf, I. Reid, S. Gould, and A. Van Den Hengel, “Vision-and-language navigation: Interpreting visually-grounded navigation instructions in real environments,” in *Proceedings of the IEEE conference on computer vision and pattern recognition*, 2018, pp. 3674–3683.
- [11] Y. Hong, Q. Wu, Y. Qi, C. Rodriguez-Opazo, and S. Gould, “Vln bert: A recurrent vision-and-language bert for navigation,” in *Proceedings of the IEEE/CVF conference on Computer Vision and Pattern Recognition*, 2021, pp. 1643–1653.
- [12] Y. Cui, L. Xie, Y. Zhang, M. Zhang, Y. Yan, and E. Yin, “Grounded entity-landmark adaptive pre-training for vision-and-language navigation,” in *Proceedings of the IEEE/CVF International Conference on Computer Vision*, 2023, pp. 12 043–12 053.
- [13] F. Giones and A. Brem, “From toys to tools: The co-evolution of technological and entrepreneurial developments in the drone industry,” *Business Horizons*, vol. 60, no. 6, pp. 875–884, 2017.
- [14] DroneII, “Drone market report,” 2024. [Online]. Available: https://droneii.com/product/drone-market-report?srsId=AfmBOor-qVivIWByTvyTvfvT_ZNWT1ZJJ7N52-1K0j_4QoQ0cImOEUI
- [15] A. D. Ames, S. Coogan, M. Egerstedt, G. Notomista, K. Sreenath, and P. Tabuada, “Control barrier functions: Theory and applications,” in *2019 18th European control conference (ECC)*. IEEE, 2019, pp. 3420–3431.
- [16] A. D. Ames, X. Xu, J. W. Grizzle, and P. Tabuada, “Control barrier function based quadratic programs for safety critical systems,” *IEEE Transactions on Automatic Control*, vol. 62, no. 8, pp. 3861–3876, 2016.
- [17] OpenAI, “Clip: Connecting text and images,” <https://github.com/openai/CLIP>, 2021.
- [18] Ultralytics, “Yolov5: Object detection at 640x640,” <https://github.com/ultralytics/yolov5>, 2020.
- [19] F. Furrer, M. Burri, M. Achtelik, and R. Siegwart, “Rotors—a modular gazebo mav simulator framework,” *Robot Operating System (ROS) The Complete Reference (Volume 1)*, pp. 595–625, 2016.
- [20] L. Yue, D. Zhou, L. Xie, F. Zhang, Y. Yan, and E. Yin, “Safe-vln: Collision avoidance for vision-and-language navigation of autonomous robots operating in continuous environments,” *IEEE Robotics and Automation Letters*, 2024.
- [21] C. Huang, O. Mees, A. Zeng, and W. Burgard, “Visual language maps for robot navigation,” in *2023 IEEE International Conference on Robotics and Automation (ICRA)*. IEEE, 2023, pp. 10 608–10 615.
- [22] Z. Wang, X. Li, J. Yang, Y. Liu, and S. Jiang, “Gridmm: Grid memory map for vision-and-language navigation,” in *Proceedings of the IEEE/CVF International Conference on Computer Vision*, 2023, pp. 15 625–15 636.
- [23] B. Lin, Y. Zhu, Z. Chen, X. Liang, J. Liu, and X. Liang, “Adapt: Vision-language navigation with modality-aligned action prompts,” in *Proceedings of the IEEE/CVF Conference on Computer Vision and Pattern Recognition*, 2022, pp. 15 396–15 406.
- [24] T. Pejša, J. Kantor, H. Benko, E. Ofek, and A. Wilson, “Room2room: Enabling life-size telepresence in a projected augmented reality environment,” in *Proceedings of the 19th ACM conference on computer-supported cooperative work & social computing*, 2016, pp. 1716–1725.
- [25] D. An, H. Wang, W. Wang, Z. Wang, Y. Huang, K. He, and L. Wang, “Etpnav: Evolving topological planning for vision-language navigation in continuous environments,” *IEEE Transactions on Pattern Analysis and Machine Intelligence*, 2024.
- [26] R. Ibrahimov, E. Tsykunov, V. Shirokun, A. Somov, and D. Tsetserukou, “Dronepick: Object picking and delivery teleoperation with the drone controlled by a wearable tactile display,” in *2019 28th IEEE International conference on robot and human interactive communication (RO-MAN)*. IEEE, 2019, pp. 1–6.
- [27] H. Abdī, G. Raja, and R. Ghabcheloo, “Safe control using vision-based control barrier function (v-cbf),” in *2023 IEEE International Conference on Robotics and Automation (ICRA)*. IEEE, 2023, pp. 782–788.
- [28] W. Xiao, T.-H. Wang, R. Hasani, M. Chahine, A. Amini, X. Li, and D. Rus, “Barriernet: Differentiable control barrier functions for learning of safe robot control,” *IEEE Transactions on Robotics*, vol. 39, no. 3, pp. 2289–2307, 2023.
- [29] M. De Sa, P. Kotaru, and K. Sreenath, “Point cloud-based control barrier function regression for safe and efficient vision-based control,” in *2024 IEEE International Conference on Robotics and Automation (ICRA)*. IEEE, 2024, pp. 366–372.
- [30] V. N. Sankaranarayanan, A. Saradagi, S. Satpute, and G. Nikolakopoulos, “A cbf-adaptive control architecture for visual navigation for uav in the presence of uncertainties,” *arXiv preprint arXiv:2402.10729*, 2024.
- [31] S. Sanyal and K. Roy, “Ramp-net: A robust adaptive mpc for quadrotors via physics-informed neural network,” in *2023 IEEE International Conference on Robotics and Automation (ICRA)*. IEEE, 2023, pp. 1019–1025.
- [32] S. Sanyal, R. K. Manna, and K. Roy, “Ev-planner: Energy-efficient robot navigation via event-based physics-guided neuromorphic planner,” *IEEE Robotics and Automation Letters*, 2024.
- [33] A. Joshi, S. Sanyal, and K. Roy, “Real-time neuromorphic navigation: Integrating event-based vision and physics-driven planning on a parrot bebop2 quadrotor,” *arXiv preprint arXiv:2407.00931*, 2024.
- [34] M. R. Fernandes, G. M. Magalhães, Y. R. C. Zúñiga, and J. B. do Val, “Gnss/mems-ins integration for drone navigation using ekf on lie groups,” *IEEE Transactions on Aerospace and Electronic Systems*, vol. 59, no. 6, pp. 7395–7408, 2023.
- [35] Tzutalin, “Labelimg,” <https://github.com/tzutalin/labelImg>, 2020.
- [36] M. S. Andersen, J. Dahl, and L. Vandenberghe, “Cvxopt: Python software for convex optimization,” <https://cvxopt.org>, 2021.
- [37] F. Furrer, M. Burri, M. Achtelik, and R. Siegwart, *Robot Operating System (ROS): The Complete Reference (Volume 1)*. Cham: Springer International Publishing, 2016, ch. RotorS—A Modular Gazebo MAV Simulator Framework, pp. 595–625.